J. Membrane Biol. 159, 169–178 (1997)

The Journal of
Membrane
Biology

Kinetic Analysis of Ca^{2+}/K^+ Selectivity of an Ion Channel by Single-Binding-Site Models

D. Gradmann[1], E. Johannes[2], U.-P. Hansen[3]

[1]Biophysical Laboratory, A.-v.-Haller-Institute for Plant Sciences, University of Göttingen, Untere Karspüle 2, D-37073 Göttingen, Germany
[2]The Plant Laboratory, Biology Department, University of York, P.O. Box 373, York YO1 5YW, UK
[3]Institut für Angewandte Physik der Universität, Olshausenstr. 40, D-24098 Kiel, Germany

Received: 19 February 1997/Revised: 19 May 1997

Abstract. Current-voltage relationships of a cation channel in the tonoplast of *Beta vulgaris*, as recorded in solutions with different activities of Ca^{2+} and K^+ (from Johannes & Sanders 1995, J. Membrane Biol. **146:**211–224), have been reevaluated for Ca^{2+}/K^+ selectivity. Since conversion of reversal voltages to permeability ratios by constant field equations is expected to fail because different ions do not move independently through a channel, the data have been analyzed with kinetic channel models instead. Since recent structural information on K^+ channels show one short and predominant constriction, selectivity models with only one binding site are assumed here to reflect this region kinetically. The rigid-pore model with a main binding site between two energy barriers (nine free parameters) had intrinsic problems to describe the observed current-saturation at large (negative) voltages. The alternative, dynamic-pore model uses a selectivity filter in which the binding site alternates its orientation (empty, or occupied by either Ca^{2+} or K^+) between the cytoplasmic side and the luminal side within a fraction of the electrical distance and in a rate-limiting fashion. Fits with this model describe the data well. The fits yield about a 10% electrical distance of the selectivity filter, located about 5% more cytoplasmic than the electrical center. For K^+ translocation, reorientation of the unoccupied binding site (with a preference of about 6:5 to face the lumenal side) is rate limiting. For Ca^{2+}, the results show high affinity to the binding site and low translocation rates (<1% of the K^+ translocation rate). With the fitted model Ca^{2+} entry through the open channel has been calculated for physiological conditions. The model predicts a unitary open channel current of about 100 fA which is insensitive to cytoplasmic Ca^{2+} concentrations (between 0.1 and 1 μM) and which shows little sensitivity to the voltage across the tonoplast.

Key words: Calcium — Channel — Current-voltage curves — Selectivity filter — Rate theory — Kinetic model

Introduction

Entry of Ca^{2+} into the cytoplasm through ion channels is an important subject in contemporary physiology. Strictly Ca^{2+}-selective channels have not been identified in plants yet. There are, however, many reports about channels in plant membranes which allow Ca^{2+} permeation to a small but sufficient extent. For a quantitative estimate of this portion, it was common usage to measure current-voltage relationships (*IV*-curves) in the presence of K^+ and Ca^{2+} and to convert the obtained reversal voltages to relative permeabilities by constant field equations (e.g., Bertl & Slayman, 1992; Johannes, Brosnan & Sanders, 1992; Ding & Pickard, 1993; Gelli & Blumwald, 1993; Piñeros & Tester, 1994; Allen & Sanders, 1995, 1996; Schulz-Lessdorf & Hedrich, 1995; Ward, Pei & Schroeder, 1995). This approach is based on the assumption of *independent* movement of different ion species (Goldman, 1943), which has been questioned to be valid for individual channels where competition between various transportees can rather be expected (Hille, 1992; Gradmann, 1996). An explicit treatment, based on rate-theory, suffered from complexity, because channels have widely been accepted to have several binding sites in series (Hille & Schwarz, 1978). This notion was mainly based on flux-coupling ratios and anomalous mole fraction effects. Nevertheless, the rigid-pore model with several binding sites (energy wells) separated by

Correspondence to: D. Gradmann

Eyring barriers, can describe superlinear (e.g., exponentially rising with driving force) *IV*-curves pretty well (e.g., White & Ridout, 1995; Gambale et al., 1996). However, because of the reaction kinetic complexity of this model (with nine states and twenty-six rate constants for two substrates and two binding sites), the obtained solutions are either equivocal or considerably restricted by simplifying assumptions such as symmetries. Furthermore, the stronghold of the rigid pore model, the anomalous mole fraction effect, turned out to be weak, because the rigid pore model cannot describe the observed voltage-sensitivity of the anomalous mole fraction effects (Draber et al., 1991). In addition, conformational changes associated with ion permeation through channels (Pietrobon, Prod'hom & Hess, 1988) render the rigid pore model unlikely.

With the concept that channel selectivity is not only a matter of ionic radii but also of ionic masses, Wu (1991) advanced a molecular model of the selectivity filter with only one binding site. This model also accounts for high flux coupling ratios and anomalous mole fraction effects. Hence, straight forward reaction kinetic treatment of channel selectivity is reasonable again. Formalisms for selectivity of charge-translocation through systems with one binding site are available for rigid pores (Hille, 1992) and for dynamic models where the binding site alternates its orientation between one side of the membrane and the other side. The latter model is currently known as carrier-model, because it was originally designed for (relatively slow) carriers (Läuger, 1973). Later (Läuger, 1980), the model has also been applied to pumps and (relatively fast) channels. Hence, the more general expression *dynamic*-model seems to be more accurate, because it bears no numerical implication about the rates.

The algorithms for selectivity of the dynamic model have been worked out already and applied for Na^+/K^+-selectivity (Gradmann, Klieber & Hansen, 1987) and Rb^+/K^+-selectivity (Klieber & Gradmann, 1993) of K^+ channels in plants. This dynamic model describes supralinear *IV*-curves rather well, e.g., current saturation for large voltage displacements, whereas the rigid-pore model fits better to nonsaturating *IV*-curves. Furthermore, a modification of the dynamic model with one binding site provides a better description of anomalous mole fraction effects than the rigid-pore model with several binding sites (Draber, Schultze & Hansen, 1991). These previous applications of the dynamic-pore model did not account, however, for recent knowledge about the molecular structure of K^+ channels (Pongs, 1992; Aiyar et al., 1995; Sun et al., 1996), according to which the narrow selectivity filter spans only a small fraction of the entire length of a wider pore.

This study presents a kinetic analysis of *IV*-curves from a tentatively Ca^{2+}-conducting cation channel (Johannes & Sanders, 1995*a*), with a dynamic selectivity filter which spans only a fraction of the entire pore length. For this purpose, the original form of the dynamic selectivity filter (Gradmann et al., 1987) with six states and twelve free parameters, has been modified by a simplification, and by an extension. The simplification reflects the assumption that binding and debinding reactions are much faster than the reorientation of the binding site. With this assumption eight rate constants can be replaced by four equilibrium constants, resulting in a reduction of free parameters by four. The extension accounts for amount and location of the electrical distance of the selectivity filter within the pore, using the ion well concept (Mitchell, 1966). With these additional two parameters the complete dynamic-pore model for channel selectivity between two transportees has ten free parameters.

For comparative purposes, the given data have also been analysed by a rigid-pore model with one binding site. This model has nine free parameters. The results render the dynamic model superior.

In principle, current saturation at large voltage displacements from equilibrium can also be due to diffusion-limitation (Laver, Fairley & Walker, 1989). In such cases, saturation currents should mainly be proportional to the concentration of the main substrate in the source compartment, i.e., luminal potassium, $[K^+]_l$, in our case. For the data analyzed here, however, the various saturation levels of K^+ currents at constant $[K^+]_l$ are rather due to inhibiting effects of a competing, second substrate, i.e., $Ca^{2+}{}_l$. Therefore, diffusion-limitation models have not been considered in our case.

Materials and Methods

Data

Experimental *IV*-curves from the open state of the predominant channel in the tonoplast of *Beta vulgaris* are taken from Johannes and Sanders (1995). The substrate concentrations, corrected for activity, in the cytoplasmic ($_c$) and luminal ($_l$) compartment were $[K^+]_c = [K^+]_l$: 38 mM, $[Ca^{2+}]_c$: <0.1 μM, and $[Ca^{2+}]_l$: 12.5, 42, 125, and 414 μM for the *IV* curves Nr. 1 to 4, respectively.

Theory

Rigid-Pore Model

The rigid-pore model (Fig. 1, left column) assumes a time-invariant energy profile along the channel for a given state of occupancy. Different ligands are expected, however, to change the profile in a specific manner. The profile at the top of column *A* in Fig. 1 illustrates the energy profile without ligand. It consists of an energy well at the electrical distance w between two barriers (heights) at the distances h_c and h_l from the boundary ($0 < h_c < w < h_l < 1$). The well corresponds to the binding site which equilibrates with competing substrates (here

K^+ and Ca^{2+}) in the bulk phases on the two sides of the membrane via rate-limiting Eyring barriers. The symbols used are marked in the two top panels of Fig. 1*A*. Let p_E, p_{EK} and p_{ECa} be the probabilities of the binding site to be empty (E), occupied by K^+ (EK^+) or occupied by Ca^{2+} (ECa^{2+}). The rate constants for binding and debinding are b_{cK}, b_{lK}, b_{cCa}, b_{lCa}, and d_{cK}, d_{lK}, d_{cCa}, d_{lCa} respectively. These rate constants depend on the transmembrane voltage V, and on the substrate concentrations in the following way

$$b_{cK} = b^0_{cK} \exp(h_c u)\ [K^+]_c \tag{1a}$$
$$d_{cK} = d^0_{cK} \exp(h_c u - w u) \tag{1b}$$
$$d_{lK} = d^0_{lK} \exp(h_l u - w u) \tag{1c}$$
$$b_{lK} = b^0_{lK} \exp(h_l u - u)\ [K^+]_l \tag{1d}$$

and for Ca^{2+}

$$b_{cCa} = b^0_{cCa} \exp(h_c u)\ [Ca^{2+}]_c \tag{2a}$$
$$d_{cCa} = d^0_{cCa} \exp(h_c u - w u) \tag{2b}$$
$$d_{lCa} = d^0_{lCa} \exp(h_l u - w u) \tag{2c}$$
$$b_{lCa} = b^0_{lCa} \exp(h_l u - u)\ [Ca^{2+}]_l \tag{2d}$$

where the superscript ^{0} marks the rate constant at zero voltage and 1 mol m^{-3} substrate concentration, and $u = VF/(RT)$ is the reduced transmembrane voltage with the voltage V, and F, R, T having the usual thermodynamic meanings.

Summarizing

$$b_K = b_{cK} + b_{lK} \tag{3a}$$
$$d_K = d_{cK} + d_{lK} \tag{3b}$$
$$b_{Ca} = b_{cCa} + b_{lCa} \tag{3c}$$
$$d_{Ca} = d_{cCa} + d_{lCa} \tag{3d}$$

and taking the determinant

$$det = b_K d_{Ca} + b_{Ca} d_K + d_K d_{Ca} \tag{4}$$

yields the mean occupancies

$$p_E = d_K d_{Ca}/det \tag{5a}$$
$$p_{EK} = b_K d_{Ca}/det \tag{5b}$$
$$p_{ECa} = b_{Ca} d_K/det \tag{5c}$$

which are used to calculate the net transport rates

$$J_K = p_E b_{cK} - p_{EK} d_{cK} \tag{6a}$$
$$J_{Ca} = p_E b_{cCa} - p_{ECa} d_{cCa} \tag{6b}$$

as well as the current

$$I = e(J_K + 2\ J_{Ca}). \tag{7}$$

with the elementary charge e.

Because of microscopic reversibility only three of the four rate constants for the translocation of an ion species are independent. In our example with two substrates and three electrical distances, this model has nine independent parameters. Without additional subtleties of diffusion limitation, the currents in this model do not saturate at large voltage displacements.

Dynamic-Pore Model

In contrast to the above rigid pore model, we call it a dynamic pore, if the energy profile of the channel — in a given state of occupancy — fluctuates. This is illustrated by the two traces in the top panel of Fig. 1*B*, in which the two energy peaks around the binding site alternate in surmounting one another. The possible role of such fluctuations for many mechanisms of ion transport has been pointed out by Läuger (1980). Binding and debinding occurs preferentially on the side of the lower energy barrier. So in our case, each of the three states of occupancy of the binding site (empty, K^+-occupied, or Ca^{2+}-occupied), can be either open to the cytoplasmic side (states 1, 3, and 5 in middle panel Fig. 1*B*, or to luminal side (states 2, 4, and 6 respectively) of the membrane.

Since the constriction of the selectivity filter in a channel spans only a small distance of the entire thickness of the membrane, the electrical width and location of the selectivity filter has to be accounted for with respect to the whole length of the pore. This has been done here with the concept of ion wells (Mitchell, 1966).

Figure 1*B* illustrates a channel with a cytoplasmic and luminal portion of the pore through which free electrodiffusion can take place, and a selectivity filter in between, the behavior of which is described here by rate theory. For a formal treatment of the model, the six states of the selectivity filter are numbered arbitrarily as illustrated. The explicit reaction scheme (*see* Klieber & Gradmann, 1993) comprises fourteen rate constants

$$k_{ij} = k^0_{ij} \exp(d_{ij} u + n_{ij}\ ln[S_{ij}])), \tag{8}$$

for transitions from state i to an adjacent state j. Here, the superscript ^{0} marks again reference conditions (zero voltage and 1 mol m^{-3} concentrations), n_{ij} is the stoichiometry for substrate binding, and d_{ij} is a voltage-sensitivity coefficient.

In the absence of an energy source (electrical or chemical gradient), the principle of microscopic reversibility requires for the two closed reaction loops

$$\frac{k^0_{12} k^0_{24} k^0_{43} k^0_{31}}{k^0_{21} k^0_{42} k^0_{34} k^0_{13}} = \frac{k^0_{43} k^0_{35} k^0_{56} k^0_{64}}{k^0_{34} k^0_{53} k^0_{65} k^0_{46}} = 1 \tag{9a,b}$$

Here the model is used with two modifications. First, according to previous investigations (Fisahn, Mikschl & Hansen, 1986; Fisahn & Hansen, 1987; Gradmann et al., 1987; Klieber & Gradmann, 1993) binding and debinding reactions can be assumed to be fast compared with the reorientation steps:

$$k_{24},\ k_{42},\ k_{31},\ k_{13},\ k_{35},\ k_{53},\ k_{46},\ k_{64} \gg k_{12},\ k_{21},\ k_{43},\ k_{34},\ k_{56},\ k_{65}. \tag{10}$$

With this relationship, the eight parameters on the left side of (3) can be reduced to four equilibrium constants

$$K_1 = k_{31}/k_{13} \tag{11a}$$
$$K_2 = k_{42}/k_{24} \tag{11b}$$
$$K_5 = k_{35}/k_{53} \tag{11c}$$
$$K_6 = k_{46}/k_{64} \tag{11d}$$

where $K_i = K^0_i[S_i]$ denotes again fundamental (K^0_i) and apparent (K_i) equilibria. With this simplification, the relative occupancies $p_1 \ldots p_6$ ($0 < p_i < 1$) of the six states can be calculated according to Klieber and Gradmann (1993) with the following auxiliary variables

$$q_3 = k_{34} + k_{21} K_2 + k_{65} K_6 \tag{12a}$$
$$q_4 = k_{34} + k_{12} K_1 + k_{56} K_5 \tag{12b}$$

and

$$r_3 = 1 + K_1 + K_5 \quad (13a)$$
$$r_4 = 1 + K_2 + K_6 \quad (13b)$$

which yield the denominator

$$d_{34} = r_3 q_3 + r_4 q_4 \quad (14)$$

which is used to calculate the occupancies

$$p_3 = q_3/d_{34} \quad (15a)$$
$$p_4 = q_4/d_{34} \quad (15b)$$
$$p_1 = p_3 K_1 \quad (15c)$$
$$p_2 = p_4 K_2 \quad (15d)$$
$$p_5 = p_3 K_5 \quad (15e)$$
$$p_6 = p_4 K_6. \quad (15f)$$

The model can account for various stoichiometries n of substrate translocation per reaction cycle. Here, only $n = 1$ is used. The empty binding site (states 3 and 4) may have the charge z_E. This yields for the occupied states 1 and 2

$$z_{EK} = z_E + n_K z_K = z_E + 1 \quad (16a)$$

and for the states 5 and 6

$$z_{ECa} = z_E + n_{Ca} z_{Ca} = z_E + 2. \quad (16b)$$

Apart from the simplification of the model of Klieber and Gradmann (1993), namely the assumption of fast binding equilibria, the following extension has been used here. The selectivity filter is assumed not to sense the entire transmembrane voltage V but only a certain fraction, Δ_s, thereof, whereas the remaining portion drops within the pore between the selectivity filter and the cytoplasmic bulk (Δ_c) and the luminal bulk (Δ_l) respectively ($\Delta_c + \Delta_s + \Delta_l = 1$). This means, that the effective substrate activities $[S_i]_{eff}$ at the binding sites of the selectivity filter are not the same as $[S_i]_b$ in the free bulk solution but

$$[S_i]_{c,eff} = [S_i]_{c,b} \exp(z_s \Delta_c u) \quad (17a)$$
$$[S_i]_{l,eff} = [S_i]_{l,b} \exp(-z_s \Delta_l u) \quad (17b)$$

according to the ion well concept of Mitchell (1966).

The rates of net translocation for K^+ and Ca^{2+} through the open channel are

$$J_K = p_1 k_{12} - p_2 k_{21}, \quad (18a)$$
$$J_{Ca} = p_5 k_{56} - p_6 k_{65}, \quad (18b)$$

and the net current

$$I = e\,[z_{EK}(p_1 k_{12} - p_2 k_{21}) + z_E(p_3 k_{34} - p_4 k_{43}) + z_{ECa}(p_5 k_{56} - p_6 k_{65})] \quad (19)$$

The entire model has ten free parameters: two of the three Δs, the two rate constants k_{34}, and k_{43}, plus three parameters (e.g., two rate constants for reorientation and one equilibrium constant, whereas the second equilibrium constant is determined by microscopic reversibility) for each of the two translocation loops.

A systematic discussion of the two models with respect to the effects of the individual parameters on the shape of the *IV*-curves, will be the subject of a separate, theoretical study.

Numerical Methods

For fitting n free model parameters to the data, a cyclic procedure was used in which each parameter was changed by multiplication and by division with an increment factor f (start usually = 1.01). The alternative which yielded the smaller *SD* was accepted and the next parameter was changed. When repetitions of these cycles did not yield better fits anymore, the increment was reduced to $f^{1/2}$ until f fell below the stop criterion (usually $f = 1.001$). This time consuming procedure has turned out to provide better multi-parameter fits than the faster Simplex algorithm from Press et al. (1987). The squareroot, *SD*, of the mean squares of the deviations between experimental data and fitted values, has been used as a measure for the fit quality. If not stated otherwise, the model was fitted to the entire bulk of data, i.e., to all four *IV*-curves from different $[Ca^{2+}]_l$ conditions.

Results and Discussion

The data from the four experimental *IV*-curves have been analyzed with the two one-binding-site models illustrated in Fig. 1. Fits with the rigid-pore-model converged readily to equivalent solutions from a wide variety of start parameters. The result is illustrated in column *A* of Fig. 2. The numerical results are listed in Table 1. Before these results are evaluated (s.b.), the fits with the dynamic-pore model are presented for comparison.

These fits with the dynamic-pore model were rather sensitive to the start parameters and converged frequently to unsatisfying solutions. On the other hand, after an *ad hoc* strategy, the fits with the dynamic-pore model were better than those with the rigid-pore model. Essential steps of the employed strategy are documented in Table 2. During the first, crude attempts, the solutions seemed to be insensitive to whether some Ca^{2+} is allowed to pass or not ($1 \gg k^0_{56}, k^0_{65} \geqslant 0$) and to whether there is a voltage drop across the selectivity filter or not ($1 \gg \Delta_s \geqslant 0$, compare lines 2_1 with 2_2, and 3_1 with 3_2 in Table 2). In cases of $\Delta_s = 0$ (no voltage across the selectivity filter), the configuration of the zs in the central six-state reaction scheme did not matter, of course. In this situation, the distances Δ_c and Δ_l were fixed to 50%, and k^0_{56}, k^0_{65}, to very small amounts (10^{-8} pAe^{-1}). So only six free parameters had to be investigated. After a few trials (*see* lines 1 to 7 in Table 2), the parameters listed in line 6_0, turned out to serve as good start parameters for visually satisfying fits (*SD* < 280 fA). With these start parameters, full ten-parameter fits to individual *IV*-curves resulted in considerably better fits (*SD*s: 165, 105, 223, and 225 fA for the *IV*-curves 1 to 4 respectively), and simultaneous fits to all four sets showed now further improvements with $1 \gg k^0_{56}, k^0_{65} > 0.01$ (lines 8 in Table 2) and with $\Delta_s > 0$ (about 10%, *see* lines 10 to 12 in Table 2). Consequently, the configuration of the zs (related on z_E of the empty binding site) had now an impact on the quality of the fits. Varying z_E in integer steps resulted in best fits with the assumption of an elec-

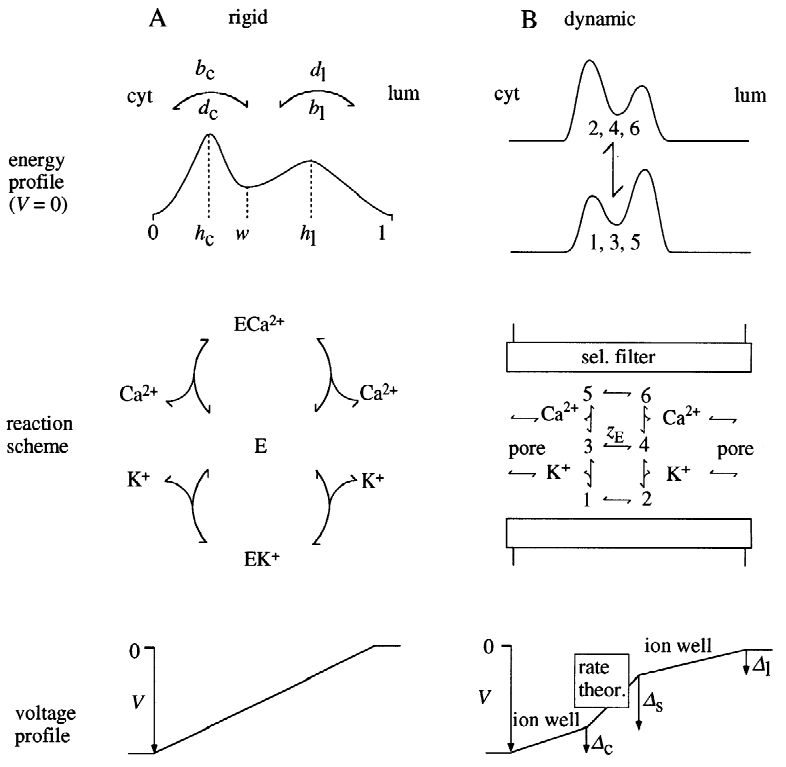

Fig. 1. Models and symbols of selectivity filter with one binding site; (*A*) rigid pore model, (*B*) dynamic pore model.

trically neutral binding site ($z_E = 0$, *see* lines 8 in Table 2). For determination of the impact of voltage profile on the fits, an eccentric position of the selectivity filter has been assumed for the start conditions. With either asymmetry in the start configuration, the fit tended toward symmetry (*see* lines 10_1 and 10_2 in Table 2). Now, with the assumption of a central position of the selectivity filter in the channel, the electrical width has been focused (lines 10_4 to 10_6 in Table 2). The best fits were obtained with a starting width of 40% ($100 - \Delta_c - \Delta_l$), which converged towards 9% (line 10_5 in Table 2). With this result, the role of the charge states has been re-examined (compare lines 10_5 and 11_i Table 2) with the result that $z_E = 0$ yielded the best fits. There is, however, no necessity to assume an integer charge of the binding site, because the essential groups can be expected to bear partial charges.

The best fits with the dynamic pore model yielded the parameters shown in Table 3 (line 10_5 in Table 2, *SD* = 263 fA). These fits are illustrated by column *B* in Fig. 2. The figures in Table 2 are not important in each detail of the eventually discarded fits; they do, however, indicate the ranges in which the individual parameters vary from approach to approach.

As for the rigid-pore model, the best fit to the ensemble of all four data sets (illustrated in column *A* of Fig. 2) was worse (*SD* = 301 fA) than the best fit with the dynamic pore model (Table 3). Furthermore, fits of the rigid-pore model to individual curves (*not shown*) turned out to be worse (*SD*s: 197, 146, 356, 297 fA for the *IV*-curves Nr. 1 to 4 respectively) than those with the dynamic-pore model (*see above*). Figure 2 illustrates, that the rigid-pore model with its nonsaturation feature has intrinsic difficulties to describe the observed current saturation at large (here negative) voltage displacements. Systematic deviations between measured and fitted *IV*-curves can be seen in Fig. 2*A*. In contrast, the dynamic-pore model fits well, i.e., without visible systematic deviations.

It should be mentioned, however, that the currents of the dynamic-pore model with the parameters listed do actually not saturate at large voltages but pass an extremum before they fall again (due to high affinity and low translocation of Ca^{2+}) — and rise again in a superlinear fashion when $k_{56}, k_{65} \gg k_{12}, k_{21}$ due $z_{ECa} > z_{EK}$. These features are not illustrated. The underlying cooperative inhibition of K^+ currents by a competing ion and *V*, has already been described in terms of the dynamic-pore model for the predominant K^+ channel in the tonoplast of *Chara*. The effect of Na^+ has first been analysed by Bertl (1989), the effect of Cs^+ in more dynamic detail by Klieber and Gradmann (1993) and by Draber and Hansen (1994). Actually, the effect of Ca^{2+} on K^+ currents has already been analyzed by Klieber and Gradmann (1993). In this previous study, however, Ca^{2+} passage through the channel was not permitted and the full membrane voltage was used for the voltage-sensitivity of the reorientation of the empty and K^+-occupied binding site,

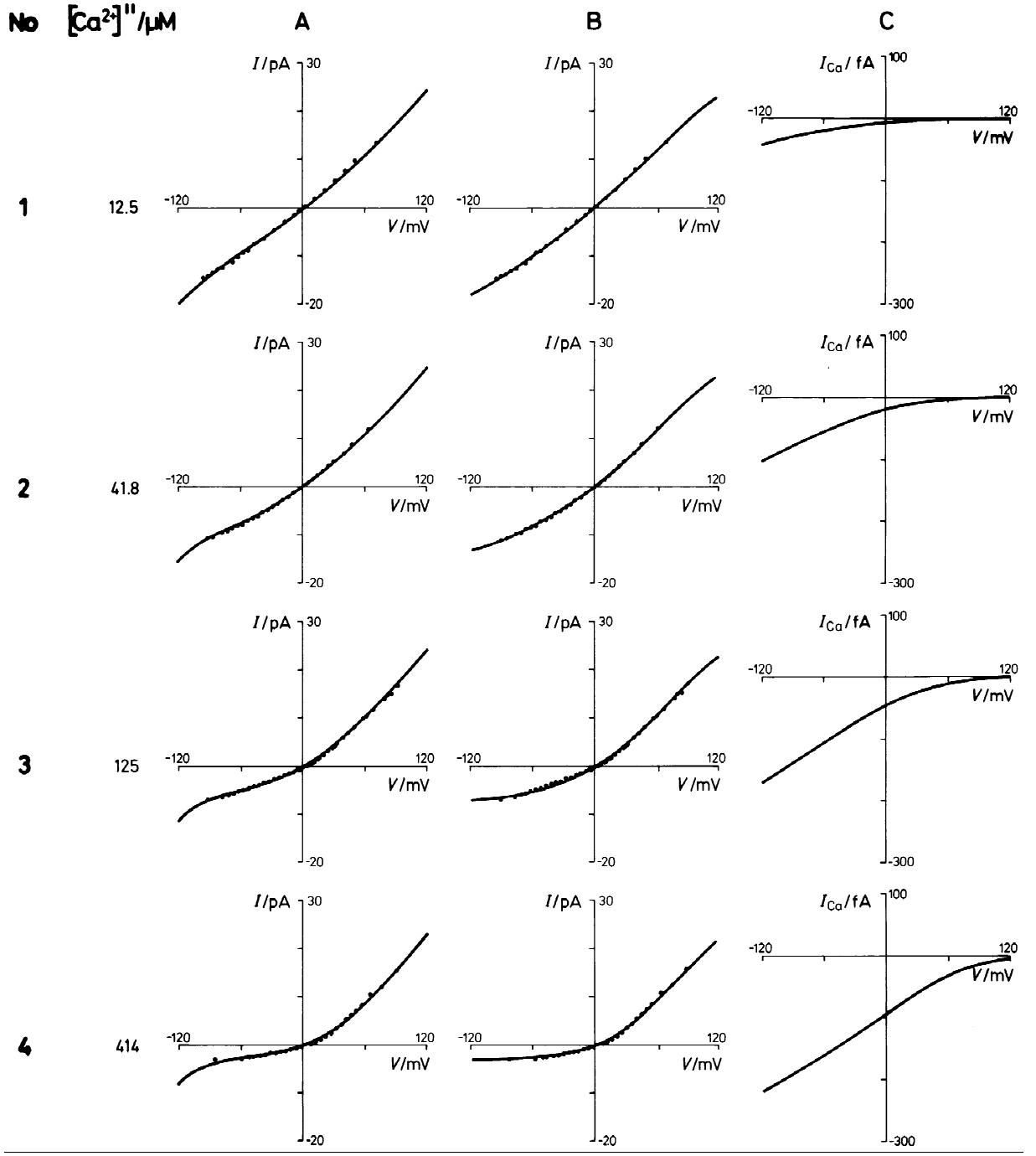

Fig. 2. Experimental data and fitted curves. Experimental conditions: $[K^+]_c = [K^+]_i = 38$ mM, $[Ca^{2+}]_c < 0.1$ µM, four different $[Ca^{2+}]_i$ as marked in second column; same data in columns *A* and *B;* column *A:* fitted by rigid pore model with parameters listed in Table 2; note tendency of fitted curves to leave saturation at large negative *V;* column *B:* fitted by dynamic filter within conducting pore (S. Fig. 1) with parameters listed in Table 3; column (*C*) Ca^{2+} currents resulting from fits by dynamic selectivity model (column *B*); note: expanded current scale.

which was justified by the strong curvatures of the *IV*-curves.

The main aim of this study, however, is presentation of the model in which a dynamic selectivity filter somewhere within the channel senses only a fraction of the membrane voltage. The present nonlinearities of the *IV*-curves of the cation channel in the *Beta* tonoplasts are not as strong as of those in *Chara.* This is reflected by the resulting, small electrical distance for the voltage drop across the selectivity filter (Table 2, lines 10_i and

Table 1. Best fit by rigid-pore model

A: Model parameters; units of rate constants (pA e^{-1}), chosen for convenient refrence to measured currents (in pA)

Param.	Amount		Unit	Physical meaning electrical distances from cytoplasm
	Fit start	Fit end		
h_c	10	32	%	Position of barrier on ctyoplasmic side
w	50	72	%	Position of well
h_l	90	79	%	Position of barrier on luminal side
				Fundamental rate constants
b^0_{cK}	0.1	0.30	pA e^{-1} mM^{-1}	Cytoplasmic K^+ binding
d^0_{cK}	0.1	46.3	pA e^{-1}	Cytoplasmic K^+ debinding
b^0_{lK}	0.1	0.28	pA e^{-1} mM^{-1}	Luminal K^+ binding
$d^{l0}{}_K$	0.1	42.9	pA e^{-1}	Luminal K^+ debinding
b^0_{cCa}	0.1	0.28	pA e^{-1} mM^{-1}	Cytoplasmic Ca^{2+} binding
d^0_{cCa}	0.1	0.07	pA e^{-1}	Cytoplasmic Ca^{2+} debinding
$b^0_{l\,Ca}$	0.1	17.2	pA e^{-1} mM^{-1}	Luminal Ca^{2+} binding
$d^0_{l\,Ca}$	0.1	4.2	pA e^{-1}	Luminal Ca^{2+} debinding
SD	6 659	309	fA	mean deviation of experimental data from fit

B: predicted Ca^{2+} currents at zero voltage

$[Ca^{2+}]_l$/μM	I_{Ca}/*fA*
12.5	−5.2
42	−16.2
125	−39
414	−79

11_i). And even this fraction may be questioned to be significant on statistical grounds.

The physical meaning of numerical results in Table 3 can be summarized as follows: The electrical distance of the selectivity filter is only about 10% of the entire membrane. It is located near the electrical center, about 5% more towards the cytoplasmic side. This electrical location can be consistent with a completely different physical location, such as in the shaker channel where the physical locus of the channel constriction is close to the luminal side but the pore is much wider on the cytoplasmic side (Antz et al., 1997).

For K^+ translocation, the limiting step in both directions is reorientation of the empty and electroneutral binding site (k_{43}, $k_{34} \ll k_{12}$, k_{21}). In the absence of driving forces the empty binding site has a slight preference to face the luminal side compared to the cytoplasmic side (k^0_{34}:$k^0_{43} \approx 6$:5). In the absence of Ca^{2+}, the binding site is mostly empty and seldom occupied by K^+ (K^0_1, $K^0_2 \ll 1$). However, once K^+ is bound, it is translocated very quickly (k^0_{12}, k^0_{21} some 10^4 pAe^{-1}). As for Ca^{2+} these features are just the opposite: high affinity and low translocation rates (K^0_5, $K^0_6 \gg 1$ mM, and k^0_{56}, k^0_{65} around 0.1 pAe^{-1}).

For the experimental conditions used, the small Ca^{2+} currents, as they result from our analysis, are illustrated by the third column of Fig. 2. It should be noticed, that the analyzed Ca^{2+} currents do not reverse their sign at the diffusion equilibrium E_{Ca}. This effect is due to partial coupling of I_{Ca} to I_K (in opposite directions) by the common transport site.

The experiments analyzed here have been carried out under conditions of about constant $[Ca^{2+}]_c < 0.1$ μM. The predictive nature of the model permits calculation of Ca^{2+} entry through this open channel also under more physiological conditions. It is of particular physiological interest, how changes in $[Ca^{2+}]_c$ will affect Ca^{2+} entry through this open channel. The results of such calculations are shown in Fig. 3, and predict a unitary open channel current of about 100 fA at 1 mM luminal Ca^{2+}. In the range of physiological $[Ca^{2+}]_c$ between 0.1 and 1 μM, the calculated Ca^{2+} influx is virtually insensitive to $[Ca^{2+}]_c$, and the assumed voltage between 0 and −60 mV across the tonoplast has also no dramatic effect on the unitary Ca^{2+} current through this open channel.

Although these Ca^{2+} currents are smaller than pseudo-permeability ratios would suggest, an individual channel would still cause an enormous load for $[Ca^{2+}]_c <$ 1 μM. It must be kept in mind, however, that the analysis carried out here refers to the open channel, and that a role

Table 2. Protocol of strategy to fit reaction scheme of rigid pore model in Fig. 1*B* with listed free parameters; bold: focused issues; k/pA e^{-1}, Δ/%, K/mM^{-1}

Nr	z_E	k^0_{34}	k^0_{43}	k^0_{12}	k^0_{21}	K^0_1	k^0_{56}	k^0_{65}	K^0_5	Δ_c	Δ_1	*SD*/fA	comment	
First trials with few parameters: Search for good start parameters and impact of voltage profile														
1_0	−2	**100**	**100**	**100**	**100**	**1**	**10^{-8}**	**10^{-8}**	**10**	**50**	**50**		(start)	
1_e	−2	36.4	75.9	91.4	605	.147	–	–	22.1	50	50	**302**	Δ fixed	
2_0	−2	**10**	**10**	**10 000**	**10 000**	**.1**	–	–	10	50	50		(start)	
2_1	−2	28.9	36.3	7 428	12 462	.077	–	–	20.9	50	50	**272**	Δ fixed	
2_2	−2	14.9	20.3	3 852	26 614	.036	–	–	10.6	43	45	279	Δ fitted	
3_0	−2	10	10	**1 000**	**1 000**	.1	–	–	10	50	50		(start)	
3_1	−2	30.4	38.3	867	1 348	.080	–	–	21.5	50	50	274	Δ fixed	
3_2	−2	15.3	23.0	487	2 476	.037	–	–	10.5	44	44	284	Δ fitted	
4_0	−2	**30**	**40**	1 000	1 000	.08	–	–	20	50	50		(start)	
4_1	−2	31.6	37.3	920	1 119	.075	–	–	22.0	50	50	273		
5_0	−2	**29**	**36**	1 000	1 000	.06	–	–	20	50	50		(start)	
5_1	−2	29.5	36.7	1 028	936	.060	–	–	20.6	50	50	276		
6_0	−2	29	36	**10 000**	**10 000**	.06	–	–	20	50	50		(start)	
6_1	−2	28.7	35.7	10 087	9 889	.057	–	–	21	50	50	272	Δ fixed	
6_2	−2	29.7	35.3	10 226	9 586	.061	–	–	21.1	50	50	**270**	Δ fitted	
7_0	−2	29	36	**100 000**	**100 000**	.06	–	–	20	50	50		(start)	
7_1	−2	28.5	35.6	100 244	99 952	.060	–	–	20.7	50	50	272	Δ fixed	
7_2	−2	29.0	36.0	100 874	100 374	.061	–	–	20.4	50	50	271	Δ fitted	
Supplement more parameters														
Allow Ca^{2+} passage													k^0_{56}, k^0_{65} (start)	
8_1	−2	37.4	33.2	12 665	8 896	.068	.93	.54	15.9	47	53	278	**1.0**	
8_2	−2	29.4	35.3	10 175	9 985	.060	.102	.097	20.7	50	50	**268**	**0.1**	
8_4	−2	28.6	33.7	10 000	9 802	.059	.010	.010	21.0	49	50	270	**0.01**	
Examine charge states														
9_1	**−1**	29.8	35.1	10 275	9 730	.061	.105	.102	21.0	50	50	267		
9_2	**0**	29.8	35.1	10 176	9 730	.061	.105	.100	21.0	50	50	**267**		
Re-examine voltage profile													Δ_c	Δ_l (start)
10_1	0	39.3	31.6	17 847	5 531	.040	.118	.094	23.1	30	50	264	**10**	**90**
10_2	0	31.2	35.8	12 278	9 292	.058	.094	.079	18.8	49	51	266	**90**	**10**
10_4	0	39.3	35.8	24 702	7 778	.044	.099	.058	16.8	37	50	272	**10**	**10**
10_3	0	40.1	33.4	17 414	7 291	.055	.101	.076	21.4	37	51	265	**20**	**20**
10_5	0	35.4	31.9	13 411	8 154	.058	.102	.082	20.1	40	51	**263**	**30**	**30**
10_6	0	31.9	32.2	11 087	8 710	.058	.109	.098	21.3	45	50	266	**40**	**40**
Re-examine charge states														
11_1	−2	20.0	51.6	9 479	8 349	.038	.086	.096	16.6	17	20	285	other: s. 10_5	
11_2	−1	26.4	23.4	7 147	10 668	.060	.097	.106	20.4	39	48	268	other: s. 10_5	
11_4	+1	34.8	38.7	10 923	9 432	.073	.107	.089	21.5	48	51	269	other: s. 10_5	

of this channel in $[Ca^{2+}]_c$ relations should be discussed more on the level of gating and channel density. Respective investigations predict a high local Ca^{2+} current when the channel is active (Johannes & Sanders, 1995*a*,*b*). However, it should be kept in mind that channel gating is difficult to measure under physiological conditions and that regulatory factors might be missing under the conditions used in the experiments. To ultimately assess the amount of Ca^{2+} which passes through the active channel, Ca^{2+} fluxes across the tonoplast need to be measured directly and correlated with the activity of the channel under investigation. This approach has been success-

Table 3. Model parameters of best fit by dynamic pore model (Fig. 1*B*); units of rate constants (pA e^{-1}), chosen for convenient reference to measured currents in pA); $z_E = 0$.

Param.	Amount	Unit	Physical meaning electrical distances:
Δ_c	40	%	From selectivity filter to cytoplasm
Δ_s	9	%	Width of selectivity filter
Δ_l	51	%	From selectivity filter to lumen
			Fundamental rate constants for reorientation:
k^0_{12}	13311	pA e^{-1}	K^+-occupied, from cytoplasm to lumen
k^0_{21}	8154	pA e^{-1}	K^+-occupied, from lumen to cytoplasm
k^0_{34}	35.4	pA e^{-1}	Empty, from lumen to cytoplasm
k^0_{43}	31.9	pA e^{-1}	Empty, from cytoplasm to lumen
k^0_{56}	0.102	pA e^{-1}	Ca^{2+}-occupied, from cytoplasm to lumen
k^0_{65}	0.082	pA e^{-1}	Ca^{2+}-occupied, from lumen to cytoplasm
			Stability constants:
K^0_1	0.058	mM^{-1}	k^0_{31}/k_{13} for state Nr. 1
K^0_2	0.085	mM^{-1}	k^0_{42}/k_{24} for state Nr. 2
K^0_5	20.1	mM^{-1}	k^0_{35}/k_{53} for state Nr. 5
K^0_6	22.5	mM^{-1}	k^0_{46}/k_{64} for state Nr. 6
SD	263	fA	Mean deviation of experimental data from fit

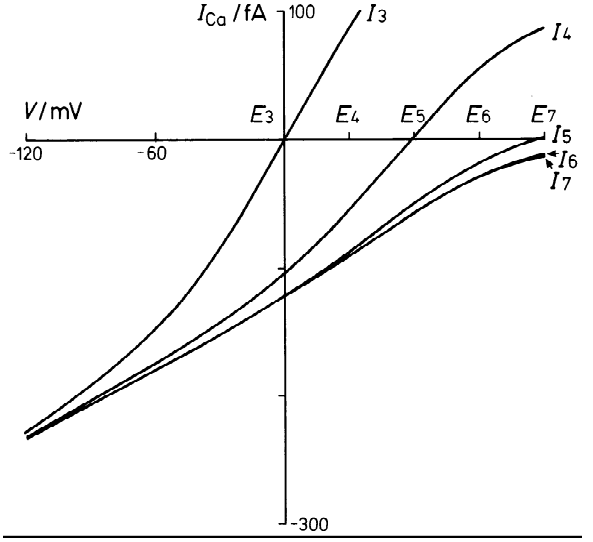

Fig. 3. Ca^{2+} currents, I_{Ca}, *vs.* tonoplast voltage, *V*, for 1 mM $[Ca^{2+}]_l$, and 0.1 μM (I_7) to 1 mM (I_3) $[Ca^{2+}]_c$, predicted by dynamic selectivity model (Fig. 1) with fitted parameters as listed in Table 3; (*E*) Nernst equilibrium voltages for Ca^{2+}, *I:* Ca^{2+} currents, indices: pCa_c; note weak sensitivity of I_{Ca} to *V*, and insensitivity of I_{Ca} to pCa_c in physiological ranges (i.e., −50 mV < V < 0 mV, and 6 < pCa_c < 7), and discrepancies between Nernst equilibrium, E_{Ca}, and reversal of I_{Ca} which are due to coupling between I_{Ca} and I_K by the selectivity filter.

fully applied to animal systems (e.g., Schneggenburger et al., 1993) but corresponding measurements for plant cells are still missing.

Conclusions

A dynamic selectivity filter with one binding site and a short electrical distance within the pore provides a good description of the effect of luminal Ca^{2+} on the K^+ currents through the Ca^{2+} permeable cation channel in the tonoplast of *Beta vulgaris*, and gives better fits than a rigid pore-model with an equivalent number of free parameters.

This study has been supported by grants from the Volkswagen-Stiftung (I/71 27) to D.G., from the British Council (313-ARC-X-96/43) to D.G., and from the Biotechnology and Biological Sciences Research Council (PDF/14) to E.J. We thank Dr. G. Thiel for valuable discussion.

References

Aiyar, J., Withka, J.M., Rizzi, J.P., Singleton, D.H., Andrews, G.C., Lin, W., Boyd, J., Hanson, D.C., Simon, M., Detlefs, B., Lee, C., Hall, J.E., Gutman, G.A., Chandy, K.G. 1995. Topology of the pore-region of a K^+ channel revealed by the NMR-derived structures of scorpion toxins. *Neuron* **15:**1169–1181

Allen, G.J., Sanders, D. 1995. Calcineurin, a type 2B protein phosphatase, modulates the Ca^{2+}-permeable slow vacuolar ion channel of stomatal guard cells. *The Plant Cell* **7:**1473–1483

Allen, G.J., Sanders, D. 1996. Control of ionic currents in guard cell vacuoles by cytosolic and luminal calcium. *Plant Journal* **10:**1055–1069

Antz, C., Geyer, M., Fakler, B., Schott, M.K., Guy, H.R., Frank, R., Ruppersberger, J.P., Kalbitzer, H.R. 1997. NMR structure of inactivation gates from mammalian voltage-dependent potassium channels. *Nature* **385:**272–275

Bertl, A. 1989. Current-voltage relationships of a sodium-sensitive potassium channel in the tonoplast of *Chara corallina. J. Membrane Biol.* **109:**9–19

Bertl, A., Slayman, C.L. 1992. Complex modulation of cation channels in the tonoplast and plasma membrane of *Saccharomyces cerevisiae:* single channel studies. *J. Exp. Biol.* **172:**271–287

Ding, J.P., Pickard, B.G. 1993. Mechanosensory calcium-selective cation channels in epidermal cells. *Plant J.* **3:**83–110

Draber, S., Hansen, U.-P. 1994. Fast single channel measurements resolve the blocking effect of Cs^+ on the K^+ channel. *Biophys. J.* **67:**120–127

Draber, S., Schultze, R., Hansen, U.-P. 1991. Patch-clamp studies on the anomalous mole fraction effect of the K^+ channel in cytoplasmic droplets of *Nitella:* an attempt to distinguish between a multi-ion-single-file pore and an enzyme kinetic model with lazy state. *J. Membrane Biol.* **123:**183–190

Fisahn, J., Hansen, U.P. 1986. The influence of temperature on a K^+-channel and on a carrier type transporter in *Nitella. J. Exp. Bot.* **37:**440–460

Fisahn, J., Mikschl, E., Hansen, U.P. 1986. Separate oscillations of the electogenic pump and of the K^+ channel in *Characean* cells as revealed by simultaneous measurement of membrane potential and of resistance. *J. Exp. Bot.* **37:**34–47

Gambale, F., Bregante, M., Stragapede, F., Cantu, A.M. 1996. Ionic channels of the sugar beet tonoplast by a multi-ion single-file permeation mechanism. *J. Membrane Biol.* **154:**69–79

Gelli, A., Blumwald, E. 1993. Calcium retrieval from vacuolar pools. Characterization of a vacuolar calcium channel. *Plant Physiol.* **102:**1139–1146

Goldman, D.E. 1943. Potential, impedance and rectification in membranes. *J. Gen. Physiol.* **27:**37–60

Gradmann, D. 1996. Selectivity of ion channels: Competitive catalysis versus independent electrodiffusion. *J. Exp. Bot.* **47:**1733–1736

Gradmann, D., Klieber H.-G., Hansen, U.-P. 1987. Reaction kinetic parameters for ion transport from steady-state current-voltage curves. *Biophys. J.* **51:**569–585

Hille, B. 1992. Ionic Channels of Excitable Membranes, 2nd ed. Sinauer, Sunderland, MA

Hille, B., Schwarz, W. 1978. Potassium channels as multi-ion single-tile pores. *J. Gen. Physiol.* **72:**409–442

Johannes, E., Brosnan, J.M., Sanders, D. 1992. Parallel pathways for intracellular Ca^{2+} release from the vacuole of higher plants. *Plant J.* **2:**97–102

Johannes, E., Sanders, D. 1995*a*. Lumenal calcium modulates unitary conductance and gating of a plant vacuole calcium release channel. *J. Membrane Biol.* **146:**211–224

Johannes, E., Sanders, D. 1995*b*. The voltage-gated Ca release channel in the vacuolar membrane of the sugar beet resides in two activity states. *FEBS Lett.* **365:**1–6

Klieber, H.G., Gradmann, D. 1993. Enzyme kinetics of the prime K^+ channel in the tonoplast of *Chara:* selectivity and inhibition. *J. Membrane Biol.* **132:**253–265

Läuger, P. 1973. Carrier-mediated ion transport. *Science* **178:**24–30

Läuger, P. 1980. Kinetic properties of ion carriers and channels. *J. Membrane Biol.* **57:**163–178

Laver, D.R., Fairley, K.A., Walker, N.A. 1989. Ion permeation in a K^+ channel in *Chara australis:* direct evidence for diffusion limitation of ion flow in a maxi-K channel. *J. Membrane Biol.* **108:**153–164

Mitchell, P.M. 1966. Chemiosmotic coupling in oxidative and photosynthetic phosphorylation. *Biol. Rev.* **41:**255–502

Okihara, K., Kiyosawa, K. 1988. Ion composition of the Chara internode. *Plant and Cell Physiol.* **29:**21–25

Pietrobon, D., Prod'hom, B., Hess, P. 1988. Conformational changes associated with ion permeation in L-type calcium channels. *Nature* **333:**373–376

Piñeros, M., Tester, M. 1994. Characterization of a voltage-dependent Ca^{2+} selective channel from wheat roots. *Planta* **195:**478–488

Pongs, O. 1992. Molecular biology of voltage-dependent potassium channels. *Physiol. Rev.* **72:**69–85

Press, W.H., Flannery, B.P., Teukolsky, S.A., Vetterling, W.T. 1987. Numerical Recipies. The Art of Scientific Computing. Cambridge University Press, Cambridge, New York, New Rochelle, Melbourne, Sidney

Schneggenburger, R., Zhu, T., Konnerth, A., Neher, E. 1993. Fractional contribution of calcium to the cation current through glutamate-receptor channels. *Neuron* **11:**133–143

Schulz-Lessdorf, B., Hedrich, R. 1995. Protons and calcium modulate-type channels in the vacuolar-lysosomal compartment—channel interaction with calmodulin inhibitors. *Planta* **197:**655–671

Sun, Z.-P., Akabas, M.H., Goulding, E.H., Karlin, A., Siegelbaum, S.A. 1996. Exposure of residues in the cyclic nucleotide gated channel pore: P region structure and function in Gating. *Neuron* **16:**141–149

Ward, J.M., Pei, Z.-M., Schroeder, J.I. 1995. Roles of ion channels in initiation of signal transduction in higher plants. *The Plant Cell* **7:**833–844

White, P.J., Ridout, M. 1995. The K channel in the plasma membrane of roots has a multi-ion-residency pore. *J. Membrane Biol.* **133:**145–160

Wu, J. 1991. Microscopic model for selective permeation in ion channels. *Biophys. J.* **60:**238–251